NANO LETTERS

pubs.acs.org/NanoLett Letter

Rapid Atomic Ordering Transformation toward Intermetallic Nanoparticles

Mingjin Cui,[⊥] Chunpeng Yang,[⊥] Sooyeon Hwang,[⊥] Boyang Li, Qi Dong, Meiling Wu, Hua Xie, Xizheng Wang, Guofeng Wang, and Liangbing Hu*

Cite This: *Nano Lett.* 2022, 22, 255−262 Read Online

ACCESS | Metrics & More | Article Recommendations | Supporting Information

ABSTRACT: Chemically ordered intermetallic nanoparticles are promising candidates for energy-related applications such as electrocatalysis. However, the synthesis of intermetallics generally requires long annealing (several hours) to achieve the ordered structure, which causes nanoparticles agglomeration and diminished performance, particularly for catalysis. Herein, we demonstrate a new rapid Joule heating approach that can synthesize highly ordered and well-dispersed intermetallic nanoparticles. As a proof-of-concept, we synthesized fully ordered Pd_3Pb intermetallic nanoparticles that feature small size distribution (~6 nm). Computational analysis of the $L1_2$ Pd_3Pb material suggests that this rapid atomic ordering transformation can be attributed to a vacancy-mediated diffusion mechanism. Moreover, the nanoparticles demonstrate excellent electrocatalytic activity and exceptional stability for the oxygen reduction reaction (ORR), retaining >95% of the current density over 10 h of chronoamperometry test with negligible structural and compositional changes. This study demonstrates a new strategy of providing a new direction for intermetallic synthesis and catalyst discovery.

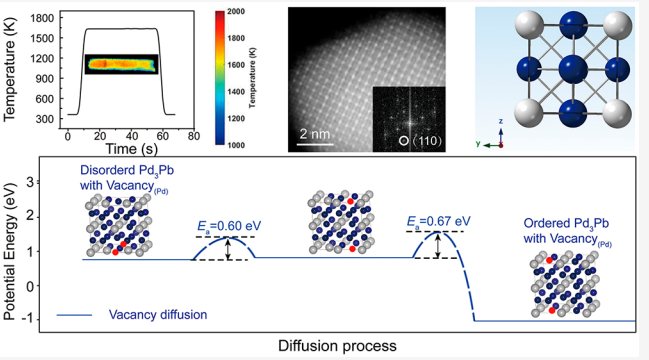

KEYWORDS: *atomic ordering, nanoparticle synthesis, intermetallic, oxygen reduction reaction*

INTRODUCTION

Intermetallic compound features well-defined stoichiometry and structural long-range ordering,[1−6] which has made these materials of great interest for applications such as catalysis,[5,7,8] magnetics,[9,10] and optical.[11] Currently, intermetallic nanoparticles are synthesized using a thermal annealing approach in which heating over a sufficient time period enables an atomic ordering transformation.[12,13] However, such long annealing processes induce particle sintering and lead to aggregation and a nonuniform size distribution, which can reduce the material's catalytic activity.[14,15] To prevent coalescence during annealing, protective nanoparticle coatings have been explored, such as silica, MgO, and Fe_3O_4 shells.[16] However, this approach requires an additional step of removing the coating from the surface of the nanoparticles[16] to expose the active sites for catalysis, which increases the cost of production and the limits practical utility. Therefore, it is critical to develop a more rapid and efficient strategy of synthesizing intermetallic nanoparticles that can also avoid aggregation issues. Recently, Chen et al. proposed the universal, ultrafast, and controllable high-temperature approach[17] to successfully realize a broad range of nanoparticle materials (such as IrNi,[18] NiO,[19] and so forth) in the diverse applications in energy storage and conversion. Ultrafast heating time can prevent an aggregation problem, but it remains extremely challenging to achieve the ordered intermetallic structure during limited heating due to the high energy barriers for the atom exchange that must take place for atomic ordering.

Here, we report a general method for the synthesis of intermetallic nanoparticles using a rapid, high-temperature heating, which not only promotes atomic ordering but also creates small and uniformly distributed particles (~6 nm). As a proof-of-concept, we synthesize Pd_3Pb intermetallic nanoparticles with a $L1_2$ structure, which we apply as an electrocatalyst for the oxygen reduction reaction (ORR).[20] By rapidly Joule heating to the temperature of 1600 K, (ramp rates on the order of 10^5 K s^{-1}), the materials decompose and then undergo an atomic ordering transformation in 60 s, which is sufficiently brief to enable the formation of ultrafine Pd_3Pb intermetallic nanoparticles (Figure 1a (i))[17] as well as $L1_2$ atomic ordering (Figure 1b). Such Joule heating at high-temperature creates numerous vacancies[21,22] in the initially disordered Pd_3Pb alloy nanoparticles, which enable the

Received: September 25, 2021
Revised: December 6, 2021
Published: December 21, 2021

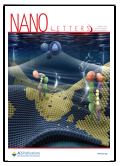

https://doi.org/10.1021/acs.nanolett.1c03714
Nano Lett. 2022, 22, 255−262

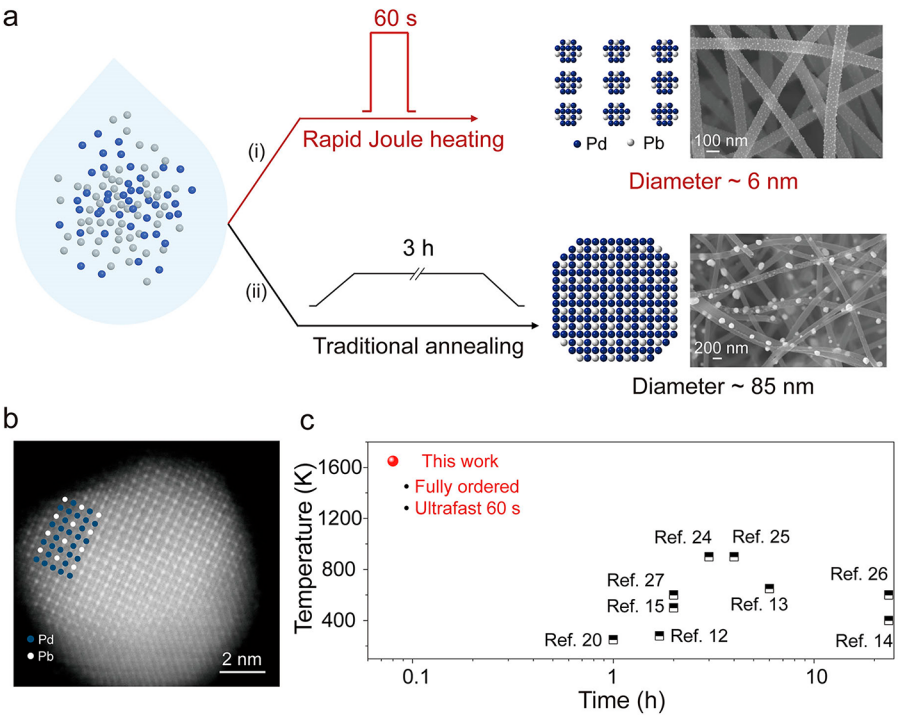

Figure 1. (a) Schematic demonstration of two strategies for the synthesis of ordered Pd_3Pb intermetallic nanoparticles from mixed Pd and Pb metal precursors: (i) the Joule heating method, which heats the materials for just 60 s at 1600 K, resulting in $L1_2$-ordered Pd_3Pb nanoparticles with an average size of ~6 nm; (ii) The traditional annealing method, which involves heating for 3 h at 1273 K, resulting in 60% ordered Pd_3Pb nanoparticles with an average size of ~85 nm. (b) A HAADF-STEM image of the resulting $L1_2$ ordered Pd_3Pb nanoparticle produced by the rapid Joule heating method. (c) Comparison of the heating temperature and time of various methods used to synthesize Pd_3Pb intermetallic nanoparticles.

elemental material to more easily rearrange into the desired ordered structure. X-ray photoelectron spectroscopy (XPS) in Figure S1 shows that the Pd 3d spectrum of Pd_3Pb has a slight shift to the lower binding energy compared to the ones in the literature.[23] The results may be attributed to the lower electron cloud density resulting from the Pd vacancies. We confirm this mechanism using density functional theory (DFT), which shows the Pd vacancy-mediated diffusion pathway has a lower activation energy (0.67 eV) compared to the nonvacancy diffusion (i.e., ring diffusion, 3.96 eV), significantly promoting the ordering processes in the $L1_2$ Pd_3Pb nanocrystal. In contrast, traditional furnace annealing featuring slow heating and long annealing time with the temperature of 1273 K results in an average intermetallic particle size of ~85 nm in Figure 1a (ii).

High-resolution high-angle annular dark-field scanning transmission electron microscopy (HAADF-STEM) image displays the periodic bright contrast due to the different *Z*-contrast of Pb (atomic number 82) and Pd (atomic number 46). As shown in Figure 1b, the HAADF-STEM image of the $L1_2$ ordered Pd_3Pb nanoparticle shows alternating layers of darker atomic columns and brighter atomic columns. Compared with previously reported intermetallic synthesis (Figure 1c),[12−15,20,24−27] the method described in this work is able to achieve an ordered structure in the 60 s by a higher temperature of 1600 K, significantly improving the ordered structure (with 100% ordering degree) in just 60 s, significantly improving the scalability of these unique materials. Furthermore, the high ordering and small particle size is vital for the catalytic activity, as we demonstrate using the Pd_3Pb intermetallic nanoparticles for ORR. Therefore, this Joule heating technique opens up a new pathway for the synthesis of intermetallic nanocatalysts for a range of applications.

As schematically shown in Figure 1a (i), to demonstrate the synthesis of intermetallic nanoparticles, we loaded metal salt precursors ($PdCl_2$ and $Pb(NO)_3$, 25 wt %, Figure S2) onto a carbon substrate (e.g., carbon nanofiber), to which we applied a voltage to enable Joule heating that can precisely control both the heating temperature and time (Figure 2a). To investigate the impact of the heating duration, we increased the temperature to 1600 K and held it for different durations (0.05, 30, and 60 s), then characterized the resulting nanoparticles on the carbon substrate using X-ray diffraction (XRD; Figure 2b). On the basis of the superlattice peaks (100) and (110) of the ordered structure, we calculated the long-range order (LRO) parameter of the samples (see definition details in Methods in Supporting Information). An intermetallic material ideally has a LRO value of 100%, indicating a full degree of atomic ordering. The XRD pattern of the Pd_3Pb nanoparticles produced by Joule heating for 0.05 s has no superlattice peaks, indicating a disordered structure (Figure 2b). Clearly, a heating time of just 0.05 s is insufficient to achieve the necessary atomic diffusion and rearrangement to form the ordered structure, instead leading to a kinetically trapped disordered materials. When we extended the heating time to 30 s, the resulting XRD spectrum featured noticeable superlattice peaks, which corresponds to a LRO value of 60%. These findings show that within 30 s of high-temperature heating a disordered−ordered phase transition occurs. Finally, when we increase the heating time increasing to 60 s, the superlattice peaks become much sharper, corresponding to a LRO value of 100%. These results show that a temperature of

https://doi.org/10.1021/acs.nanolett.1c03714
Nano Lett. 2022, 22, 255−262

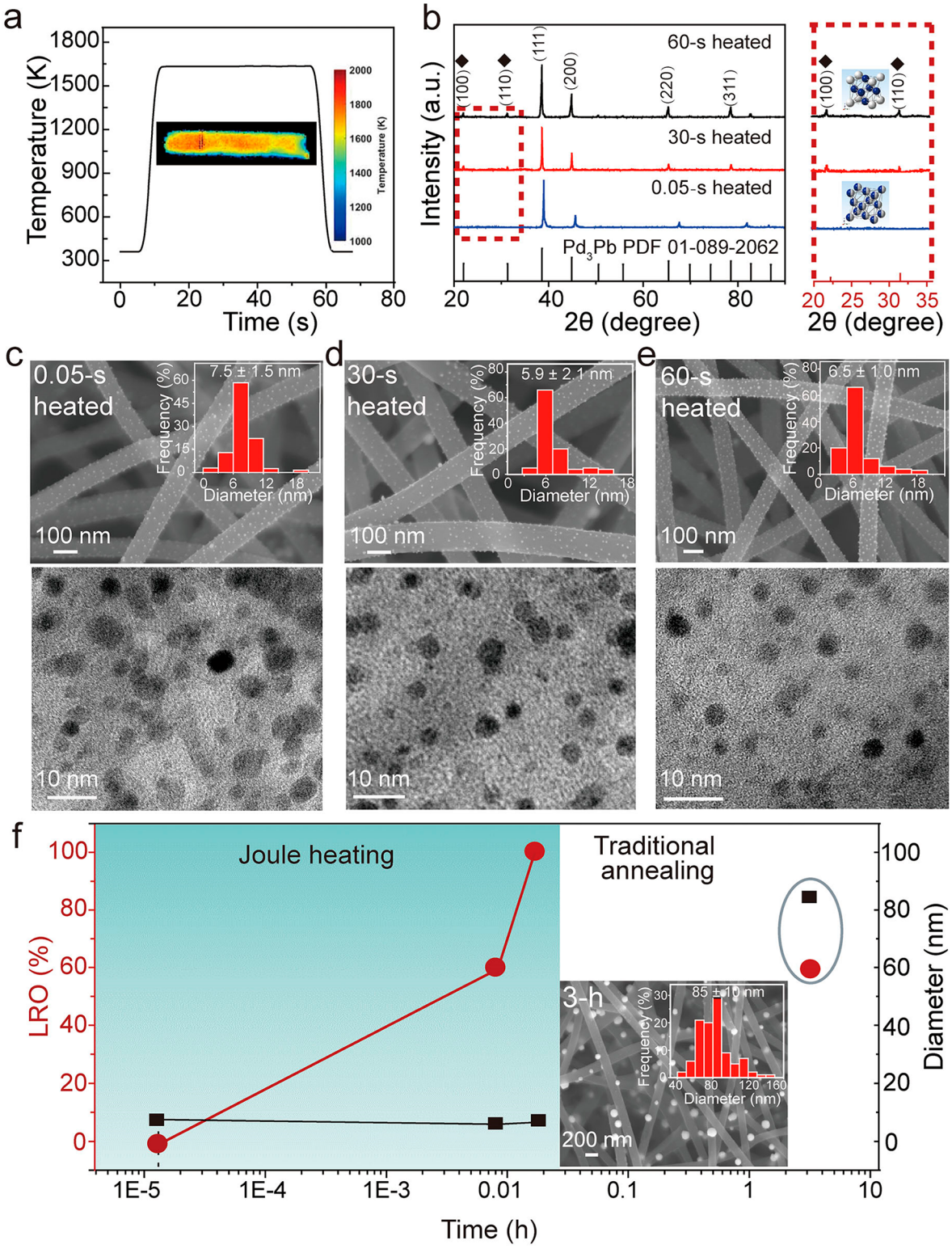

Figure 2. (a) Measurement of temperature change as a function of time during the Joule heating process. (b) XRD patterns of the Pd_3Pb nanoparticles synthesized by Joule heating at 1600 K for 0.05, 30, and 60 s, which featured disordered, 60% ordered, and 100% fully ordered structures, respectively. The superlattice peaks of (100) and (110) are marked by the black diamonds. The right plot shows an enlarged view of the spectra between 20° and 35°. The insets demonstrate the corresponding ordered (top) and disordered (bottom) structures of the Pd_3Pb lattice. (c−e) SEM and TEM images as well as the size distribution of the Pd_3Pb nanoparticles synthesized by Joule heating at 1600 K for (c) 0.05 s, (d) 30 s, and (e) 60 s. (f) LRO parameter and diameter of the Pd_3Pb nanoparticles synthesized by Joule heating for different durations (the blue shaded region part) and traditional annealing for 3 h (gray cycle part). The brown data points correspond to the LRO value (left axis) and the black data points indicate the sample diameter (right axis). The inset is an SEM image and the corresponding size distribution of the Pd_3Pb nanoparticles synthesized by the traditional annealing method (1273 K for 3 h).

https://doi.org/10.1021/acs.nanolett.1c03714
Nano Lett. 2022, 22, 255−262

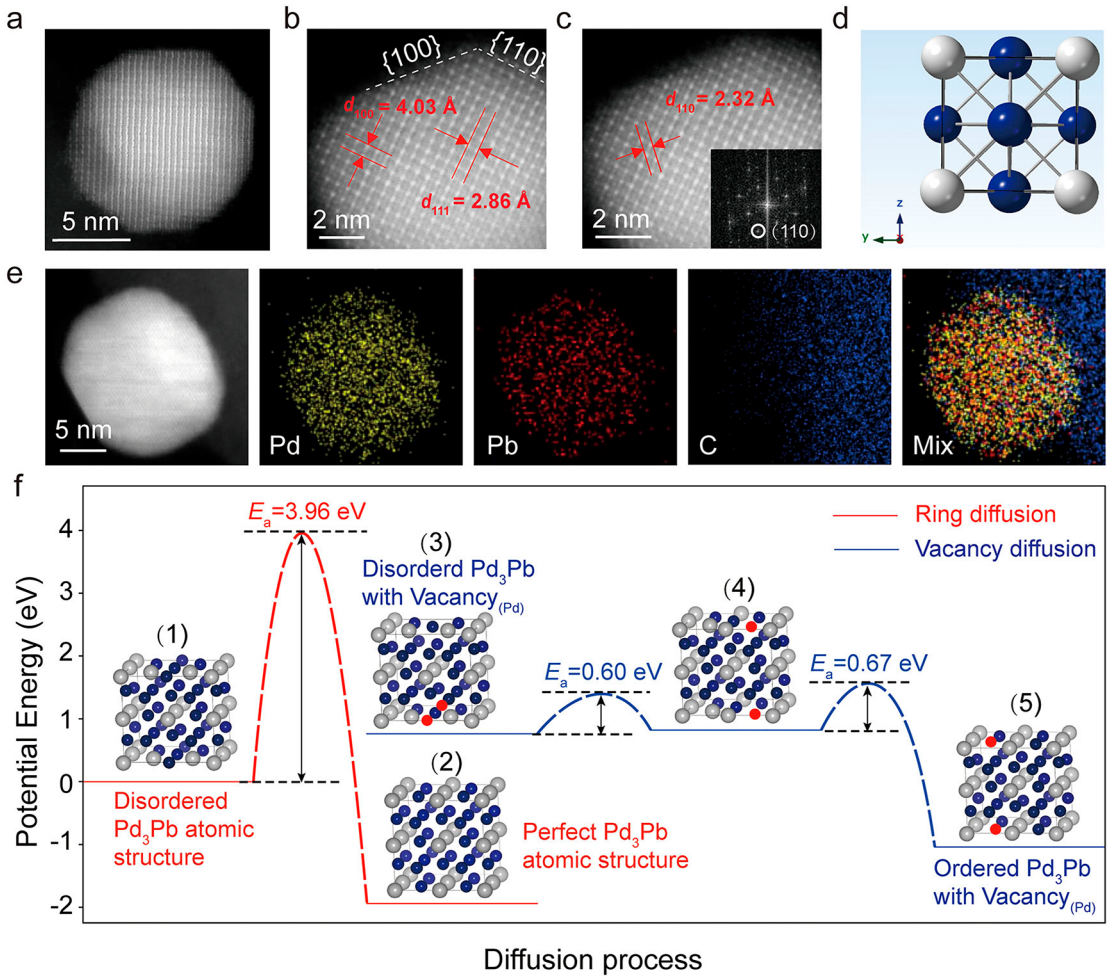

Figure 3. (a–c) HAADF-STEM images of a fully ordered Pd_3Pb nanoparticle ordered structure (a) and lattice structure (b,c) synthesized by 60 s of heating at 1600 K (the light atoms are Pd and the darker atoms are Pb). (d) Schematic of the ordered Pd_3Pb intermetallic lattice cell structure along the [001] direction. (e) HAADF-STEM image of a Pd_3Pb nanoparticle and the corresponding elemental mapping of Pd, Pb, and C, indicating the uniform distribution of the Pd and Pb elements. (f) The DFT calculation results for the atomic ordering of Pd_3Pb via the Pd vacancy diffusion (blue lines) and ring diffusion pathways (red lines). The insets are the DFT-optimized Pd_3Pb atomic structures involved in the rearrangement process. In the atomic models, the blue and gray balls represent Pd and Pb atoms, respectively. The red balls denote the Pd vacancy.

1600 K applied for 60 s can complete the disordered-to-ordered phase transition to achieve fully ordered intermetallic Pd_3Pb nanoparticles (LRO = 100%).

We investigated the impact of the Joule heating time on the size and morphology of the Pd_3Pb nanoparticles using scanning electron microscopy (SEM) and transmission electron microscopy (TEM) (Figure 2c–e). For all Joule-heating conditions (0.05, 30, and 60 s at 1600 K), the resulting Pd_3Pb nanoparticles displayed a uniform size distribution on the carbon substrate. The average sizes of the Joule heated nanoparticles were 7.5 ± 1.5, 5.9 ± 2.1, and 6.5 ± 1.0 nm corresponding to the heating time 0.05, 30, and 60 s, demonstrating a relatively narrow size distribution. In particular, the dispersion of the 60 s heated, ordered Pd_3Pb nanoparticles on the carbon substrate was uniform with no obvious aggregation. The larger size for the 60 s (6.5 nm) sample than the 30 s (5.9 nm) sample is likely due to the slight metal sintering within this short duration. It could also be a statistical result of the size-range becoming more uniform. Our study shows that 60 s Joule heating is the sufficient time to achieve intermetallic nanoparticles with high long-range ordering and ultrafine size of ∼6 nm in diameter (the blue shadow part in Figure 2f). For comparison, we also synthesized Pd_3Pb intermetallic nanoparticles using the traditional furnace annealing method at 1273 K for 3 h. The resulting materials show a lower LRO of 60% and much larger particle size of ∼85 nm (insert of Figure 2f, Figure S3). Thus, the Joule heating method is more effective for synthesizing highly ordered intermetallic nanoparticles with ultrasmall particle size.

HAADF-STEM images of the Pd_3Pb nanoparticles synthesized by 60 s Joule heating (Figure 3a–c) show the ordered structure of Pd and Pb atoms in an individual nanoparticle. The lattice fringes at 4.03, 2.32, and 2.86 Å are assigned to the (100), (111), and (110) planes of the cubic intermetallic phase of Pd_3Pb. The presence of the superlattice reflection pattern (110) also confirms the formation of the $L1_2$-ordered Pd_3Pb intermetallic structure (inset of Figure 3c). Figure 3d shows a schematic of the ordered Pd_3Pb intermetallic lattice cell structure along the [001] direction. Additionally, energy-dispersive spectroscopy (EDS) mapping shows the Pd and Pb are uniformly distributed within the Pd_3Pb nanoparticles (Figure 3e).

Vacancy diffusion and ring diffusion are two possible mechanisms that could explain the transition of the Pd_3Pb

https://doi.org/10.1021/acs.nanolett.1c03714
Nano Lett. 2022, 22, 255−262

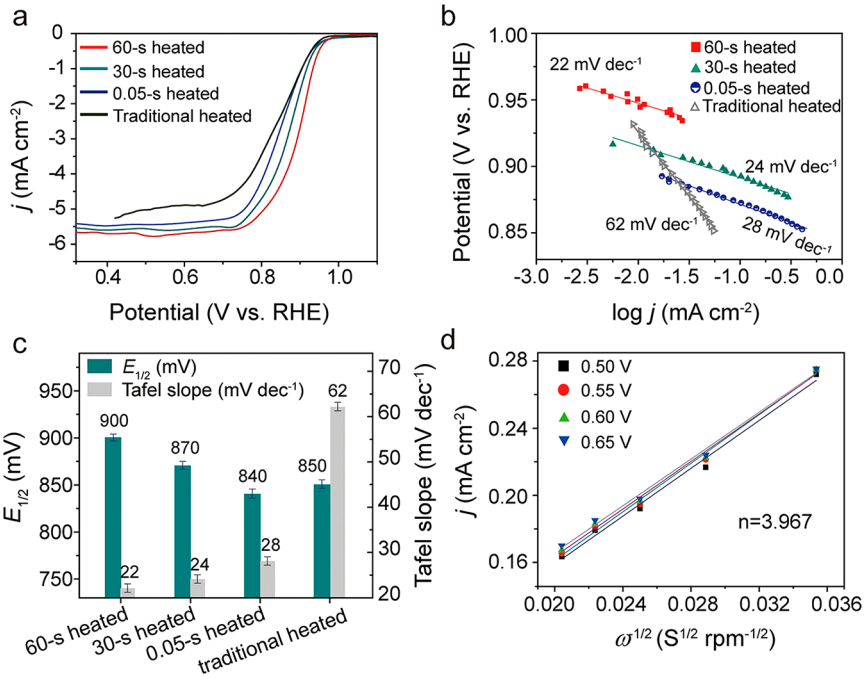

Figure 4. (a) ORR polarization curves of the 60 s heated, 30 s heated, and 0.05 s heated in O_2-saturated 1 M KOH solution (rotation rate 1600 rpm). (b) Tafel curves derived from (a). (c) Bar plots of the $E_{1/2}$ and Tafel slope values of the different heated Pd_3Pb nanoparticles. (d) The K-L plots at different electrode potentials (0.50, 0.55, 0.60, and 0.65 V) for 60 s heated sample.

nanoparticles from a disordered solid solution to an ordered crystal (Figure S4).[28] In the vacancy diffusion pathway, the vacancy swaps its position with an adjacent atom, as shown in Figure S4a. In contrast, atoms change their positions in a simultaneous direction in the ring diffusion (Figure S4b,c). Rapid Joule heating to high temperature can increase the concentration of vacancies in order for the nanoparticles to reach thermal equilibrium.[22] Therefore, in our process we hypothesize the vacancy diffusion mechanism dominates the structural ordering process of the $L1_2$ Pd_3Pb nanoparticles.

To test this hypothesis, we performed first-principles density functional theory (DFT) simulation to better understand how vacancies affect the diffusion energetics of the metal atoms during the Joule-heating-induced atomic ordering. In Figure 3f, we constructed a partially disordered Pd_3Pb model containing two pairs of disordered Pd and Pb atoms, which we used to calculate the vacancy diffusion paths toward the formation of the $L1_2$ Pd_3Pb structure. Specifically, we assumed the activation energy for the diffusion path involved a pre-existing Pd vacancy and Pb vacancy, as shown in Figure 3f and Figure S5, respectively. For comparison, we also simulated the ring diffusion process (i.e., diffusion without a vacancy in the partially disordered Pd_3Pb structure; Figure 3f(1,2) and Figure S5) in which the two pairs of Pb and Pd atoms swap their position. For this path, we calculated the activation energy to be 3.96 eV, which is insurmountable at 1600 K.[29] In contrast, we found the ordering process of the partially disordered Pd_3Pb structure featuring Pd vacancies (red dots in structure Figure 3f(3)) can overcome the two surmountable energy barriers (0.60 and 0.67 eV) via the vacancy diffusion path (Figure 3f(3−5)) in which Pb or Pd atoms swap their position with an adjacent vacancy in a step-by-step manner.

Moreover, we found the activation energies through the Pb vacancy diffusion path features three activation energy barriers, the highest of which is 1.04 eV, as shown in Figure S5, higher than Pd vacancy diffusion (0.67 eV) but much lower than the ring diffusion (3.96 eV). These results suggest vacancy diffusion is more energetically feasible for the atomic ordering of the Pd_3Pb intermetallic structure, whereas the ring diffusion mechanism is negligible due to its unsurmountable energy barrier even under the high temperature conditions used. Furthermore, we calculated the formation energy of the Pb vacancy in Pd_3Pb to be 2.07 eV, whereas the Pd vacancy exhibited a much lower formation energy of 0.76 eV, likely owing to its smaller atomic radius of Pd (140 pm < 180 pm of Pb) that results in smaller lattice distortion. Via this vacancy-mediated process, the high-concentration of vacancies generated due to the rapid heating should significantly accelerate the atom diffusion process in the crystalline state, reducing the atomic ordering transformation time scale.

Given the ultrasmall size and fully ordered intermetallic structure, the 60 s heated Pd_3Pb nanoparticles may be an excellent nanocatalyst for ORR. Figure 4a presents the ORR polarization curves of the 60 s heated Pd_3Pb nanoparticles in 1 M KOH solution saturated with oxygen, measured using a rotating disk electrode (RDE) at room temperature. The less ordered 0.05 and 30 s heated samples are also shown for comparison. The fully ordered 60 s heated Pd_3Pb exhibits a more positive half-wave potential ($E_{1/2}$, 0.90 V, vs a reversible hydrogen electrode) than the 0.05 s heating (0.84 V), and 30 s heating (0.87 V) heated materials. Compared with the 0.05 s heating sample, the $E_{1/2}$ of the 60 s heated material shows a significant 60 mV shift to more positive potentials, indicating better activity of the fully ordered intermetallic catalyst (Figure 4a). We also evaluated the performance of the catalysts (0.05 s heated, 30 s heated, and 60 s heated) by the kinetic current (j_k) versus the electrode potential. As shown in Figure 4b, the Tafel slope of the 60 s heated sample (22 mV dec^{-1}) is lower than that of 30 s heated (28 mV dec^{-1}), and 0.05 s heated (34 mV dec^{-1}) Pd_3Pb nanoparticles, indicating the superior ORR

https://doi.org/10.1021/acs.nanolett.1c03714
Nano Lett. 2022, 22, 255−262

kinetics and activity of the 60 s heated catalyst.[30] The higher activity of the intermetallic prepared by Joule heating can be attributed to the vacancies in the intermetallic nanoparticles. The vacancies can play an important role in modifying the electronic structure and the properties of nanoparticles by introducing additional energy levels. These factors could lead to the enhanced catalytic activity when used as a catalyst. The bar plot in Figure 4c summarizes the favorable ORR activity of the 60 s heated nanocatalyst in which the $E_{1/2}$ and Tafel slopes outperform the less ordered heated Pd_3Pb nanoparticles in addition to significantly exceeding that of the large Pd_3Pb particles synthesized by traditional furnace annealing.

As the heated Pd_3Pb samples are approximately the same size, but feature different degrees of atomic ordering, we attribute the superior performance of the 60 s heated sample to its fully ordered intermetallic structure. Figure S6 presents the rotation rate-dependent ORR polarization curves of the 60 s heated catalyst, which reflects first-order reaction kinetics relative to the dissolved oxygen concentration during the ORR process.[31,32] To determine the efficiency of the ORR reaction, we calculated the average electron transfer number (n) of the 60 s heated nanocatalyst within the potential range of 0.50−0.65 V from the slope of the Koutecky−Levich (K-L) plots (Figure 4d). We found n equals 3.967, indicating a nearly 4-electron reduction process of oxygen to water, which is critical for high efficiency in ORR. To investigate the electrochemically active surface area (ECSA), we measured the capacitance of the 60 and 0.05 s heating nanoparticles. According to the current density at different scan rates (from 1 to 50 mV s^{-1}) of the 60 s heated nanoparticles, the calculated double layer capacitance (C_{dl}, Figure S7) was 66.0 mF cm^{-2}, which is larger than that of the disordered 0.05 s heated nanoparticles (44.7 mF cm^{-2}). On the basis of the results of C_{dl}, the ECSA of the 60 s heated nanoparticles (78.2 m^2 g^{-1}) exceeded that of the 0.05 s heated nanoparticles (43.1 m^2 g^{-1}), which we attribute to the material's well-defined ordered structure, producing abundant active sites for the electrocatalytic process. The mass and specific activities of the most active catalyst (Figure S8), 60 s heated Pd_3Pb, are 0.59 mA mg_{Pd}^{-1} and 1.53 mA cm^{-2}, respectively, which are 2.7 and 1.2 times higher than those of the traditionally heated Pd_3Pb.

We measured the electrochemical stability of the 60 s heated Pd_3Pb intermetallic catalyst using an accelerated durability test (ADT) conducted by cycling the potential between 0.6 and 1.0 V at 50 mV s^{-1} at room temperature. As shown in Figure 5a, the 60 s heated catalyst demonstrates a slightly improved $E_{1/2}$ value after 3000 cycles of ADT (from 0.90 to 0.91 V, and undergoes negligible decay in the diffusion-limiting current. The slight improved $E_{1/2}$ value is likely a result of a higher amount of active sites on the surface of the ordered Pd_3Pb intermetallic nanoparticles due to the migration of vacancies from bulk to the surface during testing. Moreover, chronoamperometry measurements at 0.70 V of the fully ordered 60 s heated Pd_3Pb sample showed the catalyst retained up to 95% of its original current (Figure 5b). Electrochemical impedance spectroscopy (EIS) of the materials also displays negligible change before and after the long-term stability chronoamperometry test (Figure 5c). The ordered structure and the overall morphology of the 60 s heated catalyst were also maintained after chronoamperometry stability testing, as evidenced by the post-mortem XRD and SEM characterization (Figure 5d). The superior stability of the 60 s heating catalyst is mainly due to the stronger heteroatomic Pd−Pb bond in

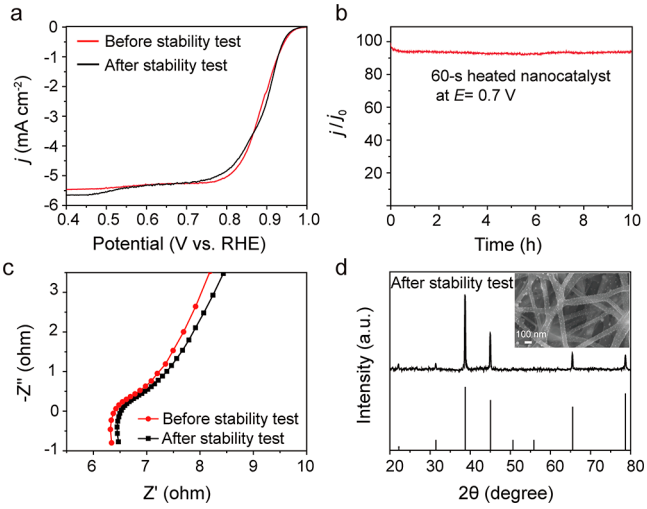

Figure 5. (a) The first and after 3000 cycles accelerated cyclic voltammetry (CV) of the 60 s heated nanocatalyst in ORR conducted at 50 mV s^{-1}. (b) Chronoamperometry of the 60 s heated nanocatalysts at 0.7 V in O_2 saturated 1 M KOH in terms of the percentage of the retained current as a function of the operation time. (c) EIS of the 60 s heated nanocatalyst before and after 3000 accelerated CV cycles conducted at 50 mV s^{-1}. (d) XRD pattern of the 60 s heated nanocatalyst after 3000 accelerated CV cycles. The inset is an SEM image of the 60 s heated nanocatalysts after the stability test (3000 cycles).

Pd_3Pb intermetallic than the randomly mixed Pd_3Pb alloy (see detailed XPS analysis in Figure S9). In contrast, under the same conditions the disordered 0.05 s heated sample showed inferior performance with lower $E_{1/2}$ and higher Tafel slope values for ORR compared with the 60 s heated (Figure S10a).

On the basis of the slope of the K-L plots, the average electron transfer number (n) of the 0.05 s heated catalyst within the potential range of 0.50−0.65 V was 3.422 (Figure S10a), which is less than that of the 60 s heated sample (n = 3.967), indicating a lower efficiency for ORR. Additionally, after a 3000 cycle stability test the disordered 0.05 s heated material also suffered from severe performance decay (Figure S10b) and particle aggregation (Figure S10c). Furthermore, the traditionally annealed Pd_3Pb nanoparticles show a dramatic decrease in activity (Figure S11a) and obvious aggregation and deterioration (Figure S11b) after the durability tests compared with the 60 s heated intermetallic rapidly synthesized by our approach.

CONCLUSION

In summary, we have demonstrated a new technique (within 60 s) for the synthesis of ordered intermetallic nanoparticles via rapid Joule heating. This high-temperature synthesis creates sufficient atomic vacancies that promote structural ordering into $L1_2$ Pd_3Pb nanocrystals. Additionally, the short heating time prevents particle aggregation, enabling ultrasmall nanoparticle size and a narrow size distribution (~6 nm). Computational analysis suggests the diffusion mechanism during the structural ordering process involves vacancies, which feature the lower activation energy for atomic diffusion compared to ring diffusion. Electrochemical experiments also show the fully ordered Pd_3Pb nanoparticles exhibit excellent electrocatalytic activity and superior stability for ORR, demonstrating only 5% of its original current degradation and negligible structural and compositional changes over 10 h

https://doi.org/10.1021/acs.nanolett.1c03714
Nano Lett. 2022, 22, 255−262

of chronoamperometry. This study presents an effective approach to enable the synthesis of intermetallics with small particle size for catalysis applications.

■ ASSOCIATED CONTENT

Supporting Information

The Supporting Information is available free of charge at https://pubs.acs.org/doi/10.1021/acs.nanolett.1c03714.

Experimental methods; additional data on XPS characterization, TGA analysis, XRD characterization; schematic of the proposed diffusion mechanism; DFT calculation diffusion process; additional data on ORR performance for materials (PDF)

■ AUTHOR INFORMATION

Corresponding Author

Liangbing Hu − *Department of Materials Science and Engineering and Center for Materials Innovation, University of Maryland, College Park, Maryland 20742, United States;* orcid.org/0000-0002-9456-9315; Email: binghu@umd.edu

Authors

Mingjin Cui − *Department of Materials Science and Engineering, University of Maryland, College Park, Maryland 20742, United States*

Chunpeng Yang − *Department of Materials Science and Engineering, University of Maryland, College Park, Maryland 20742, United States;* orcid.org/0000-0001-7075-3356

Sooyeon Hwang − *Center for Functional Nanomaterials, Brookhaven National Laboratory, Upton, New York 11973, United States;* orcid.org/0000-0001-5606-6728

Boyang Li − *Department of Mechanical Engineering & Materials Science, University of Pittsburgh, Pittsburgh, Pennsylvania 15261, United States*

Qi Dong − *Department of Materials Science and Engineering, University of Maryland, College Park, Maryland 20742, United States*

Meiling Wu − *Department of Materials Science and Engineering, University of Maryland, College Park, Maryland 20742, United States*

Hua Xie − *Department of Materials Science and Engineering, University of Maryland, College Park, Maryland 20742, United States*

Xizheng Wang − *Department of Materials Science and Engineering, University of Maryland, College Park, Maryland 20742, United States*

Guofeng Wang − *Department of Mechanical Engineering & Materials Science, University of Pittsburgh, Pittsburgh, Pennsylvania 15261, United States;* orcid.org/0000-0001-8249-4101

Complete contact information is available at: https://pubs.acs.org/10.1021/acs.nanolett.1c03714

Author Contributions

L.H., M.C., and C.Y. designed the experiments. M.C. and C.Y. carried out the materials synthesis. S.H. provided characterization via STEM. B.L. and G.W. were responsible for the density functional theory calculations. X.W. measured the temperature of the carbon substrate during Joule heating. M.C., C.Y., and L.H., collectively wrote the paper. All authors commented on the final manuscript.

Author Contributions

$^{\perp}$M.C., C.Y., and S.H. contributed equally to this work.

Notes

The authors declare no competing financial interest.

■ ACKNOWLEDGMENTS

We acknowledge the support of the Maryland Nanocenter, its Surface Analysis Center and AIMLab. We would like to thank Dylan Kline and Michael R. Zachariah at the University of Maryland, College Park for their assistance with the MATLAB coding for the high-temperature Joule heating measurement. The electron microscopy work used resources at the Center for Functional Nanomaterials, which is a U.S. DOE Office of Science Facility, at Brookhaven National Laboratory under Contract No. DE-SC0012704. B.L. and G.W. gratefully acknowledge the financial support from the National Science Foundation (NSF) (DMR 1905572) and the computational resources provided by the University of Pittsburgh Center for Research Computing.

■ REFERENCES

(1) Kim, S.-H.; Kim, H.; Kim, N. J. Brittle Intermetallic Compound Makes Ultrastrong Low-Density Steel with Large Ductility. *Nature* **2015**, *518* (7537), 77−79.

(2) Yan, Y.; Du, J. S.; Gilroy, K. D.; Yang, D.; Xia, Y.; Zhang, H. Intermetallic Nanocrystals: Syntheses and Catalytic Applications. *Adv. Mater.* **2017**, *29* (14), 1605997.

(3) Yang, T.; Zhao, Y. L.; Tong, Y.; Jiao, Z. B.; Wei, J.; Cai, J. X.; Han, X. D.; Chen, D.; Hu, A.; Kai, J. J.; Lu, K.; Liu, Y.; Liu, C. T. Multicomponent Intermetallic Nanoparticles and Superb Mechanical Behaviors of Complex Alloys. *Science* **2018**, *362* (6417), 933−937.

(4) Sankar, M.; Dimitratos, N.; Miedziak, P. J.; Wells, P. P.; Kiely, C. J.; Hutchings, G. J. Designing Bimetallic Catalysts for a Green and Sustainable Future. *Chem. Soc. Rev.* **2012**, *41* (24), 8099−8139.

(5) Wang, D. L.; Xin, H. L. L.; Hovden, R.; Wang, H. S.; Yu, Y. C.; Muller, D. A.; DiSalvo, F. J.; Abruna, H. D. Structurally Ordered Intermetallic Platinum-Cobalt Core-Shell Nanoparticles with Enhanced Activity and Stability as Oxygen Reduction Electrocatalysts. *Nat. Mater.* **2013**, *12* (1), 81−87.

(6) Yang, Y. S.; Chen, C. C.; Scott, M. C.; Ophus, C.; Xu, R.; Pryor, A.; Wu, L.; Sun, F.; Theis, W.; Zhou, J. H.; Eisenbach, M.; Kent, P. R. C.; Sabirianov, R. F.; Zeng, H.; Ercius, P.; Miao, J. W. Deciphering Chemical Order/Disorder and Material Properties at the Single-Atom Level. *Nature* **2017**, *542* (7639), 75−79.

(7) Ji, X. L.; Lee, K. T.; Holden, R.; Zhang, L.; Zhang, J. J.; Botton, G. A.; Couillard, M.; Nazar, L. F. Nanocrystalline Intermetallics on Mesoporous Carbon for Direct Formic Acid Fuel Cell Anodes. *Nat. Chem.* **2010**, *2* (4), 286−293.

(8) Gilroy, K. D.; Ruditskiy, A.; Peng, H. C.; Qin, D.; Xia, Y. N. Bimetallic Nanocrystals: Syntheses, Properties, and Applications. *Chem. Rev.* **2016**, *116* (18), 10414−10472.

(9) Clarke, S. M.; Walsh, J. P. S.; Amsler, M.; Malliakas, C. D.; Yu, T.; Goedecker, S.; Wang, Y. B.; Wolverton, C.; Freedman, D. E. Discovery of a Superconducting Cu-Bi Intermetallic Compound by High-Pressure Synthesis. *Angew. Chem., Int. Ed.* **2016**, *55* (43), 13446−13449.

(10) Amsler, M.; Naghavi, S. S.; Wolverton, C. Prediction of Superconducting Iron-Bismuth Intermetallic Compounds at High Pressure. *Chem. Sci.* **2017**, *8* (3), 2226−2234.

(11) Kim, M.; Freeman, A. J.; Kim, S.; Perepezko, J. H.; Olson, G. B. Phase Stability of the Intermetallic $L2_1$ Heusler Alloys of $A_2(Hf_{1-x}Zr_x)Al$ (where A = Pd and Pt) for an Nb-based High-Temperature Materials Design. *Appl. Phys. Lett.* **2005**, *87* (26), 261908.

(12) Kim, D.; Xie, C. L.; Becknell, N.; Yu, Y.; Karamad, M.; Chan, K.; Crumlin, E. J.; Norskov, J. K.; Yang, P. D. Electrochemical Activation of CO_2 through Atomic Ordering Transformations of AuCu Nanoparticles. *J. Am. Chem. Soc.* **2017**, *139* (24), 8329−8336.

(13) Liu, M. M.; Zhang, Z. H.; Okejiri, F.; Yang, S. Z.; Zhou, S. H.; Dai, S. Entropy-Maximized Synthesis of Multimetallic Nanoparticle Catalysts via a Ultrasonication-Assisted Wet Chemistry Method under Ambient Conditions. *Adv. Mater. Interfaces* **2019**, *6* (7), 1900015.
(14) Cui, Z. M.; Chen, H.; Zhao, M. T.; DiSalvo, F. J. High-performance Pd_3Pb intermetallic catalyst for electrochemical oxygen reduction. *Nano Lett.* **2016**, *16* (4), 2560−2566.
(15) Xiao, W. P.; Lei, W.; Gong, M. X.; Xin, H. L.; Wang, D. L. Recent Advances of Structurally Ordered Intermetallic Nanoparticles for Electrocatalysis. *ACS Catal.* **2018**, *8* (4), 3237−3256.
(16) Chung, D. Y.; Jun, S. W.; Yoon, G.; Kwon, S. G.; Shin, D. Y.; Seo, P.; Yoo, J. M.; Shin, H.; Chung, Y.-H.; Kim, H.; Mun, B. S.; Lee, K.-S.; Lee, N.-S.; Yoo, S. J.; Lim, D.-H.; Kang, K.; Sung, Y.-E.; Hyeon, T. Highly Durable and Active PtFe Nanocatalyst for Electrochemical Oxygen Reduction Reaction. *J. Am. Chem. Soc.* **2015**, *137* (49), 15478−15485.
(17) Chen, Y. N.; Egan, G. C.; Wan, J. Y.; Zhu, S. Z.; Jacob, R. J.; Zhou, W. B.; Dai, J. Q.; Wang, Y. B.; Danner, V. A.; Yao, Y. G.; Fu, K.; Wang, Y. B.; Bao, W. Z.; Li, T.; Zachariah, M. R.; Hu, L. B. Ultra-fast self-assembly and stabilization of reactive nanoparticles in reduced graphene oxide films. *Nat. Commun.* **2016**, *7*, 12332.
(18) Yao, Y.; Huang, Z.; Li, T.; Wang, H.; Liu, Y.; Stein, H. S.; Mao, Y.; Gao, J.; Jiao, M.; Dong, Q.; Dai, J.; Xie, P.; Xie, H.; Lacey, S. D.; Takeuchi, I.; Gregoire, J. M.; Jiang, R.; Wang, C.; Taylor, A. D.; Shahbazian-Yassar, R.; Hu, L. High-throughput, combinatorial synthesis of multimetallic nanoclusters. *Proc. Natl. Acad. Sci. U. S. A.* **2020**, *117* (12), 6316−6322.
(19) Liu, C.; Zhou, W.; Zhang, J. F.; Chen, Z. L.; Liu, S. L.; Zhang, Y.; Yang, J. X.; Xu, L. Y.; Hu, W. B.; Chen, Y. N.; Deng, Y. D. Air-Assisted Transient Synthesis of Metastable Nickel Oxide Boosting Alkaline Fuel Oxidation Reaction. *Adv. Energy Mater.* **2020**, *10* (46), 2001397.
(20) Bu, L. Z.; Shao, Q.; Pi, Y. C.; Yao, J. L.; Luo, M. C.; Lang, J. P.; Hwang, S.; Xin, H. L.; Huang, B. L.; Guo, J.; Su, D.; Guo, S. J.; Huang, X. Q. Coupled s-p-d Exchange in Facet-Controlled Pd3Pb Tripods Enhances Oxygen Reduction Catalysis. *Chem.* **2018**, *4* (2), 359−371.
(21) Liang, J. S.; Ma, F.; Hwang, S.; Wang, X. X.; Sokolowski, J.; Li, Q.; Wu, G.; Su, D. Atomic Arrangement Engineering of Metallic Nanocrystals for Energy-Conversion Electrocatalysis. *Joule* **2019**, *3* (4), 956−991.
(22) Wurschum, R.; Farber, P.; Dittmar, R.; Scharwaechter, P.; Frank, W.; Schaefer, H. E. Thermal Vacancy Formation and Self-Diffusion in Intermetallic Fe_3Si Nanocrystallites of Nanocomposite Alloys. *Phys. Rev. Lett.* **1997**, *79* (24), 4918−4921.
(23) Yu, X. T.; Luo, Z. S.; Zhang, T.; Tang, P. Y.; Li, J. S.; Wang, X.; Llorca, J.; Arbiol, J.; Liu, J. F.; Cabot, A. Stability of Pd_3Pb Nanocubes during Electrocatalytic Ethanol Oxidation. *Chem. Mater.* **2020**, *32* (5), 2044−2052.
(24) Du, X. X.; He, Y.; Wang, X. X.; Wang, J. N. Fine-Grained and Fully Ordered Intermetallic PtFe Catalysts with Largely Enhanced Catalytic Activity and Durability. *Energy Environ. Sci.* **2016**, *9* (8), 2623−2632.
(25) Wang, Z. X.; Yao, X. Z.; Kang, Y. Q.; Miao, L. Q.; Xia, D. S.; Gan, L. Structurally Ordered Low-Pt Intermetallic Electrocatalysts toward Durably High Oxygen Reduction Reaction Activity. *Adv. Funct. Mater.* **2019**, *29* (35), 1902987.
(26) DeSario, D. Y.; DiSalvo, F. J. Ordered Intermetallic Pt-Sn Nanoparticles: Exploring Ordering Behavior across the Bulk Phase Diagram. *Chem. Mater.* **2014**, *26* (8), 2750−2757.
(27) Kim, D.; Xie, C. L.; Becknell, N.; Yu, Y.; Karamad, M.; Chan, K.; Crumlin, E. J.; Norskov, J. K.; Yang, P. D. Electrochemical Activation of CO_2 through Atomic Ordering Transformations of AuCu Nanoparticles. *J. Am. Chem. Soc.* **2017**, *139* (24), 8329−8336.
(28) Nakajima, H.; Sprengel, W.; Nonaka, K. Diffusion in intermetallic compounds. *Intermetallics* **1996**, *4*, S17.
(29) Norskov, J. K.; Studt, F.; Abild-Pedersen, F.; Bligaard, T. *Fundamental Concepts in Heterogeneous Catalysis*; John Wiley & Sons, 2014; Vol. 7, p 196.
(30) Anderson, A. B.; Albu, T. V. Ab Initio Determination of Reversible Potentials and Activation Energies for Outer-Sphere Oxygen Reduction to Water and the Reverse Oxidation Reaction. *J. Am. Chem. Soc.* **1999**, *121* (50), 11855−11863.
(31) Liu, Q.; Jin, J. T.; Zhang, J. Y. $NiCo_2S_4$@graphene as a Bifunctional Electrocatalyst for Oxygen Reduction and Evolution Reactions. *ACS Appl. Mater. Interfaces* **2013**, *5* (11), 5002−5008.
(32) Huang, Y. P.; Miao, Y. E.; Lu, H. Y.; Liu, T. X. Hierarchical $ZnCo_2O_4$@$NiCo_2O_4$ Core-Sheath Nanowires: Bifunctionality towards High-Performance Supercapacitors and the Oxygen-Reduction Reaction. *Chem. - Eur. J.* **2015**, *21* (28), 10100−10108.

https://doi.org/10.1021/acs.nanolett.1c03714
Nano Lett. 2022, 22, 255−262